Water Hammer Mitigation via PDE-constrained Optimization [1]

Tehuan Chen[a], Chao Xu[a,2], Qun Lin[b], Ryan Loxton[b], Kok Lay Teo[b]

[a] *State Key Laboratory of Industrial Control Technology and Institute of Cyber-Systems & Control, Zhejiang University, Hangzhou, Zhejiang 310027, China.*
[b] *Department of Mathematics & Statistics, Curtin University, Perth, Western Australia 6102, Australia.*

Abstract

This paper considers an optimal boundary control problem for fluid pipelines with terminal valve control. The goal is to minimize pressure fluctuation during valve closure, thus mitigating water hammer effects. We model the fluid flow by two coupled hyperbolic PDEs with given initial conditions and a boundary control governing valve actuation. To solve the optimal boundary control problem, we apply the control parameterization method to approximate the time-varying boundary control by a linear combination of basis functions, each of which depends on a set of decision parameters. Then, by using variational principles, we derive formulas for the gradient of the objective function (which measures pressure fluctuation) with respect to the decision parameters. Based on the gradient formulas obtained, we propose a gradient-based optimization method for solving the optimal boundary control problem. Numerical results demonstrate the capability of optimal boundary control to significantly reduce pressure fluctuation.

Keywords: Water hammer, Hyperbolic PDEs, Control parameterization, Optimal boundary control, Method of lines, Variational method

1. Introduction

When gases and liquids are transported over long distances through networked pipelines, flow impulses and periodic excitations often induce unwanted transient dynamics. Such transient dynamics can adversely affect working performance, and can

---

even destroy key components in the pipeline network, through the generation of fluid-structure interactive vibration and noise. Water hammer, also known as hydraulic shock, is one of the most common transient dynamics in pipelines. It is caused by sudden changes in the motion state, such as a complete halt or a reversal of flow direction. The pressure wave caused by water hammer is the main reason for pipeline noise and vibration. Mitigation strategies for water hammer are numerous and here we refer to just a few, such as those for oil pipelines [36], air compressor pipelines [18], spacecraft propulsion systems [17], heat exchange systems in nuclear reactors [12, 32] and even cardiovascular flow in human blood vessels [28].

This paper models water hammer mitigation by an optimal boundary control problem governed by hyperbolic PDEs [8]. We consider the benchmark pipeline system shown in Figure 1, where a pipeline of length L is used to transport fluid from a reservoir to a terminus. In the literature, fluid flow is typically modeled using the well-known Navier-Stokes equations; related control studies include mixing, stabilization, and optimal shape design [5, 1]. For pipelines, the simplified version of the full Navier-Stokes model is commonly used to analyze and mitigate water hammer phenomena. This simplified model, known as the pipeline transmission PDE model, is defined by the following nonlinear hyperbolic PDE system [15, 35]:

$$\frac{\partial v}{\partial t} + \frac{1}{\rho}\frac{\partial p}{\partial l} + \frac{f}{2D}v|v| = 0, \tag{1a}$$

$$\frac{\partial p}{\partial t} + \rho c^2 \frac{\partial v}{\partial l} = 0, \tag{1b}$$

where $l \in [0, L]$ is the spatial variable, $t \in [0, T]$ is the time variable, $v = v(l, t)$ is the flow velocity, $p = p(l, t)$ is the pressure drop, D is the diameter of the pipeline, c is the wave velocity, f is the Darcy-Weisbach friction factor, and ρ is the flow density. This model is also widely used to simulate hydraulic dynamics in irrigation canals [25, 16, 21].

The initial conditions for system (1) are

$$p(l, 0) = \bar{p}_0(l), \quad v(l, 0) = \bar{v}_0(l), \quad l \in [0, L], \tag{2}$$

where $\bar{p}_0(l)$ and $\bar{v}_0(l)$ are given functions describing the initial pressure and velocity profiles. Moreover, the boundary conditions are given by

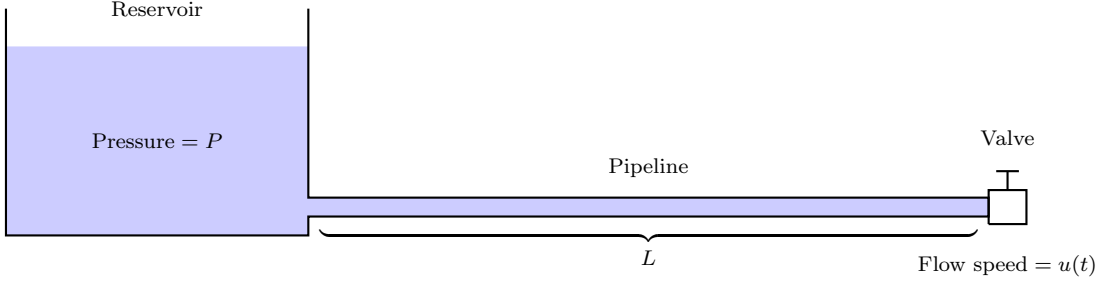$$p(0, t) = P, \quad v(L, t) = u(t), \quad t \in [0, T], \tag{3}$$

2

Figure 1: General layout of the pipeline system

where P is the pressure generated by the reservoir, and $u(t)$ is a boundary control function. System (1)-(3) is called the state system. Note that $u(t) = 0$ corresponds to a closed valve (zero flow velocity), and $u(t) = u_{\max}$ corresponds to a completely open valve (maximum flow velocity). Since the valve is initially fully open,

$$u(0) = u_{\max}. \tag{4}$$

Moreover, since the valve is required to be closed at the terminal time $t = T$, we impose the following terminal constraint:

$$u(T) = 0. \tag{5}$$

Finally, to ensure that the valve is not re-opened during the time horizon, we have the following derivative constraint:

$$\dot{u}(t) \leq 0, \quad t \in [0, T]. \tag{6}$$

Shutting off the valve suddenly will cause an oscillating pressure wave (i.e., water hammer) to propagate through the pipeline at high speed [7]. This pressure fluctuation must be controlled to avoid serious pipeline damage [3, 30]. Thus, for the pipeline system shown in Figure 1, our goal is to choose a continuous boundary control $u(t)$, in accordance with constraints (4)-(6), to minimize the following objective function as proposed in [4] for open channel flows:

$$J(u) = \frac{1}{T} \int_0^T \left[\frac{p(L,t) - \hat{p}(L)}{\bar{P}} \right]^{2\gamma} dt + \frac{1}{LT} \int_0^T \int_0^L \left[\frac{p(l,t) - \hat{p}(l)}{\bar{P}} \right]^{2\gamma} dl dt, \tag{7}$$

where γ is a positive integer, $\bar{P}$ is a given constant, $\hat{p}(l)$ is a given function expressing the target pressure profile along the pipeline and $p(l,t)$ is the solution of the state system (1)-(3). Our optimal boundary control problem is thus stated as: Given the system (1) with

3

initial conditions (2) and boundary conditions (3), choose the boundary control $u(t)$ to minimize the objective function (7) subject to the initial condition (4), the terminal control constraint (5) and the derivative constraint (6). This problem is referred to as Problem P_0.

In reference [8], we developed a discretize-then-optimize computational approach for solving Problem P_0. This approach involves first using the finite-difference method to approximate the PDE model (1)-(3) by a system of ODEs, then applying control parameterization [31] to approximate the boundary control by a piecewise-linear or piecewise-quadratic function. We call this approach the CP-ODE approach, as it involves using control parameterization to solve a conventional ODE optimal control problem, which is obtained from the original PDE problem via the finite-difference method.

In this paper, we propose an alternative computational approach in which control parameterization is applied directly to the original PDE model. We refer to this new approach as the CP-PDE approach. The advantage of CP-PDE over CP-ODE is that one layer of approximation is removed: Problem P_0 is solved directly using control parameterization; there is no need to first approximate it by a conventional ODE optimal control problem. Both CP-PDE and CP-ODE yield finite-dimensional optimization problems that can be solved using sequential quadratic programming (SQP) methods. For CP-PDE, finite-difference methods are used in conjunction with SQP to solve the PDE model; for CP-ODE, Runge-Kutta methods are used to solve the approximating ODE system. See Figure 2 for a comparison of the two approaches. Our simulation results indicate that CP-PDE requires significantly less computational effort than CP-ODE, thus motivating the new approach.

Because of the nonlinear friction term in (1), the pipeline transmission PDE system belongs to the class of semi-linear systems. Such systems have been widely studied in the literature. For example, Riemann invariants are applied in [10] to provide feedback laws for local stability using a Lyapunov function. LaSalle's invariance principle [2] has also been applied to yield asymptotic stability conditions for semi-linear systems. Note that water hammer mitigation can be viewed as a boundary stabilization problem for the pipeline transmission PDEs. In addition to our new computational optimal control framework, feedback stabilization techniques, including the Lyapunov method [9, 11],

4

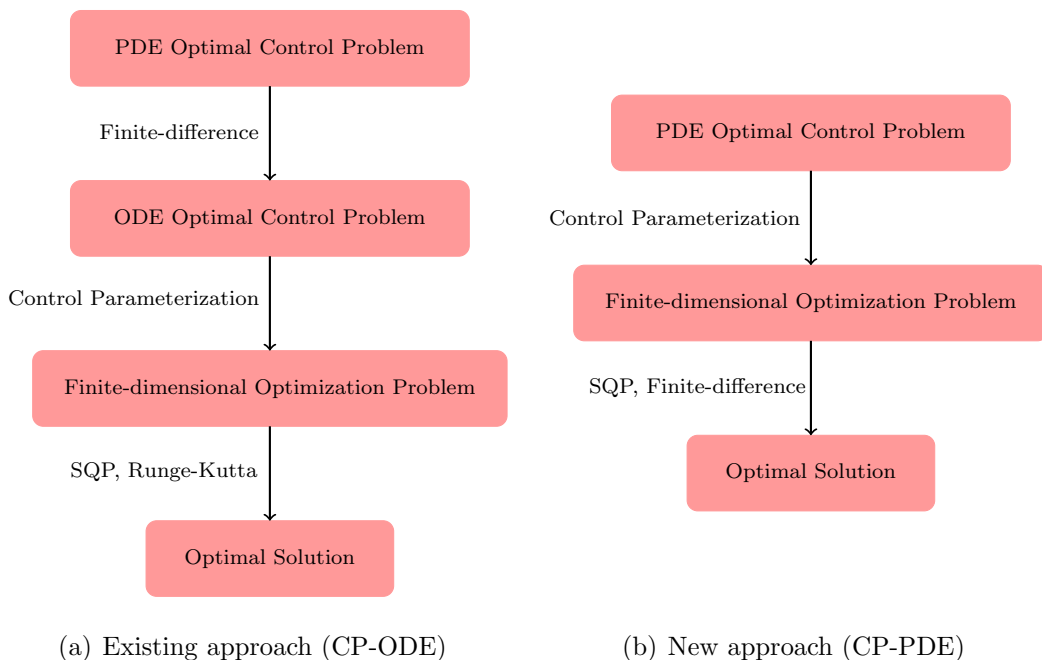(a) Existing approach (CP-ODE) (b) New approach (CP-PDE)

Figure 2: Comparing the existing approach in [8] with the new approach described in this paper

the infinite-dimensional backstepping technique [33], and a receding horizon optimal control method [29], have also been applied to the pipeline transmission PDE system for open channel flows.

The organization of this paper is described as follows. In Section 2, we introduce the control parameterization method for approximating the boundary control by a linear combination of basis functions. Also in Section 2, we derive formulas for computing the objective function's gradient with respect to the optimization parameters defining the control approximation. These formulas depend on the solution of an auxiliary set of PDEs called the costate system. In Section 3, we use the method of lines to develop numerical procedures for solving both the state system and the costate system. These procedures can be combined with standard gradient-based SQP methods to solve the approximate optimization problem derived in Section 2. In Section 4, we apply the computational approach described in Sections 2 and 3 to an example problem. Simulation results comparing CP-PDE and CP-ODE are reported. Finally, Section 5 concludes the paper with summary comments and suggestions for future research.

2. Control Parameterization

To solve Problem P_0, we approximate the boundary control $u(t)$ as follows:

$$u(t) \approx u^N(t) = \sum_{k=1}^{N} \varphi_k(t, \boldsymbol{\sigma}^k), \tag{8}$$

where $\varphi_k : \mathbb{R} \times \mathbb{R}^s \to \mathbb{R}$, $k = 1, \ldots, N$, are given basis functions, $s - 1$ is the basis function order (for example, $s = 2$ for piecewise-linear basis functions), and $\boldsymbol{\sigma}^k \in \mathbb{R}^s$, $k = 1, \ldots, N$, are parameter vectors to be optimized. In the standard control parameterization method, the two most popular choices for the basis functions are piecewise-constant basis functions and piecewise-linear basis functions [19]. However, for pipeline flow control, piecewise-constant basis functions are not appropriate because they yield a discontinuous control signal. Thus, in this paper, we use piecewise-linear and piecewise-quadratic basis functions. These basis functions are defined precisely later in this section.

Under the approximation (8), the objective function (7) can be written as follows:

$$J^N(\boldsymbol{\sigma}) = \frac{1}{T} \int_0^T \left[\frac{p^N(L,t) - \hat{p}(L)}{\bar{P}} \right]^{2\gamma} dt + \frac{1}{LT} \int_0^T \int_0^L \left[\frac{p^N(l,t) - \hat{p}(l)}{\bar{P}} \right]^{2\gamma} dl\,dt, \tag{9}$$

where $p^N(l,t)$ denotes the solution of system (1)-(3) with $u(t) = u^N(t)$, and

$$\boldsymbol{\sigma} = \left[(\boldsymbol{\sigma}^1)^\top, \ldots, (\boldsymbol{\sigma}^N)^\top \right]^\top \in \mathbb{R}^{Ns}.$$

Furthermore, the initial and terminal constraints (4) and (5) become, respectively,

$$\sum_{k=1}^{N} \varphi_k(0, \boldsymbol{\sigma}^k) = u_{\max}, \quad \sum_{k=1}^{N} \varphi_k(T, \boldsymbol{\sigma}^k) = 0. \tag{10}$$

Finally, the derivative constraint (6) becomes

$$\sum_{k=1}^{N} \frac{\partial \varphi_k(t, \boldsymbol{\sigma}^k)}{\partial t} \leq 0, \quad t \in [0, T]. \tag{11}$$

Thus, under the control approximation (8), in which $u(t)$ is restricted to the form $u^N(t)$, we obtain the following finite-dimensional optimization problem: choose the control parameter vector $\boldsymbol{\sigma}$, in accordance with constraints (10) and (11), to minimize the objective function (9). We refer to this problem as Problem P_0^N.

As we will show later, constraints (11) reduce to a finite number of linear inequality constraints for piecewise-linear and piecewise-quadratic basis functions. In some applications, it may be necessary to consider more general nonlinear control constraints in the following form:

$$h(t, u(t)) \geq 0, \quad t \in [0, T].$$

Under approximation (8), these constraints become

$$h(t, \varphi(t, \boldsymbol{\sigma}^1) + \cdots + \varphi(t, \boldsymbol{\sigma}^N)) \geq 0, \quad t \in [0, T].$$

In general, unlike (11), these constraints cannot be converted into simple linear constraints. Nevertheless, they can be handled using the penalty methods in [22, 24, 20].

2.1. Gradient Computation

To solve Problem P_0^N using nonlinear optimization algorithms, we need the gradient of the objective function (9) with respect to the control parameter vector $\boldsymbol{\sigma}$. Computing this gradient, however, is a major challenge, as the objective function depends on $\boldsymbol{\sigma}$ implicitly through the hyperbolic state system (1)-(3). The following result, which is proved using variational methods [31, 27, 34], gives formulas for computing the required gradient.

Theorem 1. *The gradient of the objective function in Problem P_0^N is given by*

$$\nabla_{\boldsymbol{\sigma}^k} J^N(\boldsymbol{\sigma}) = \rho c^2 \int_0^T \mu(L, t) \frac{\partial \varphi_k(t, \boldsymbol{\sigma}^k)}{\partial \boldsymbol{\sigma}^k} dt, \quad k = 1, \ldots, N, \tag{12}$$

where $\mu(L, t)$ is obtained by solving the following costate system:

$$\frac{f}{D} \lambda(l, t) |v^N(l, t)| - \frac{\partial \lambda(l, t)}{\partial t} - \rho c^2 \frac{\partial \mu(l, t)}{\partial l} = 0, \tag{13a}$$

$$\frac{2\gamma}{LT\bar{P}^{2\gamma}} (p^N(l, t) - \hat{p}(l))^{2\gamma - 1} - \frac{1}{\rho} \frac{\partial \lambda(l, t)}{\partial l} - \frac{\partial \mu(l, t)}{\partial t} = 0, \tag{13b}$$

with the boundary conditions

$$\mu(0, t) = 0, \quad \lambda(L, t) = -\frac{2\rho\gamma}{T\bar{P}^{2\gamma}} (p^N(L, t) - \hat{p}(L))^{2\gamma - 1}, \quad t \in [0, T], \tag{14}$$

and the terminal conditions

$$\mu(l, T) = \lambda(l, T) = 0, \quad l \in [0, L]. \tag{15}$$

Note that $\mu(l, t)$ and $\lambda(l, t)$ are the Lagrange multipliers (or costates) for Problem P_0^N.

7

Proof. Let $\alpha : [0, L] \times [0, T] \to \mathbb{R}$ denote an arbitrary Lagrange multiplier function. Furthermore, let $H_1(l, t)$ denote the left-hand side of (1a):

$$H_1(l, t) = \frac{\partial v(l, t)}{\partial t} + \frac{1}{\rho} \frac{\partial p(l, t)}{\partial l} + \frac{f}{2D} v(l, t) |v(l, t)|.$$

Then

$$\int_0^T \int_0^L \alpha(l, t) H_1(l, t) dl dt = \int_0^T \int_0^L \alpha(l, t) v_t(l, t) dl dt + \frac{1}{\rho} \int_0^T \int_0^L \alpha(l, t) p_l(l, t) dl dt$$
$$+ \frac{f}{2D} \int_0^T \int_0^L \alpha(l, t) v(l, t) |v(l, t)| dl dt.$$

Using integration by parts,

$$\int_0^T \int_0^L \alpha(l, t) H_1(l, t) dl dt = \int_0^L \{\alpha(l, T) v(l, T) - \alpha(l, 0) v(l, 0)\} dl$$
$$+ \frac{1}{\rho} \int_0^T \{\alpha(L, t) p(L, t) - \alpha(0, t) p(0, t)\} dt$$
$$+ \int_0^T \int_0^L \left\{ \frac{f}{2D} \alpha(l, t) v(l, t) |v(l, t)| - \alpha_t(l, t) v(l, t) - \frac{1}{\rho} \alpha_l(l, t) p(l, t) \right\} dl dt.$$

Since $v(l, 0) = \bar{v}_0(l)$ and $p(0, t) = P$, this equation can be simplified to give

$$\int_0^T \int_0^L \alpha(l, t) H_1(l, t) dl dt = \int_0^L \{\alpha(l, T) v(l, T) - \alpha(l, 0) \bar{v}_0(l)\} dl$$
$$+ \frac{1}{\rho} \int_0^T \{\alpha(L, t) p(L, t) - P\alpha(0, t)\} dt$$
$$+ \int_0^T \int_0^L \left\{ \frac{f}{2D} \alpha(l, t) v(l, t) |v(l, t)| - \alpha_t(l, t) v(l, t) - \frac{1}{\rho} \alpha_l(l, t) p(l, t) \right\} dl dt.$$

Hence, since $H_1(l, t) = 0$ for any pair of state trajectories $p(l, t)$ and $v(l, t)$, we have

$$\int_0^L \{\alpha(l, T) v(l, T) - \alpha(l, 0) \bar{v}_0(l)\} dl + \frac{1}{\rho} \int_0^T \{\alpha(L, t) p(L, t) - P\alpha(0, t)\} dt$$
$$+ \int_0^T \int_0^L \left\{ \frac{f}{2D} \alpha(l, t) v(l, t) |v(l, t)| - \alpha_t(l, t) v(l, t) - \frac{1}{\rho} \alpha_l(l, t) p(l, t) \right\} dl dt = 0. \tag{16}$$

To continue, let $\beta : [0, L] \times [0, T] \to \mathbb{R}$ denote another Lagrange multiplier function, and define $H_2(l, t)$ as the left-hand side of (1b):

$$H_2(l, t) = \frac{\partial p(l, t)}{\partial t} + \rho c^2 \frac{\partial v(l, t)}{\partial l}.$$

Then again by using integration by parts,

$$\int_0^T \int_0^L \beta(l,t) H_2(l,t) dldt = \int_0^T \int_0^L \beta(l,t) p_t(l,t) dldt + \rho c^2 \int_0^T \int_0^L \beta(l,t) v_l(l,t) dldt$$

$$= \int_0^L \left\{ \beta(l,T) p(l,T) - \beta(l,0) p(l,0) \right\} dl$$

$$- \int_0^T \int_0^L \left\{ \beta_t(l,t) p(l,t) + \rho c^2 \beta_l(l,t) v(l,t) \right\} dldt$$

$$+ \rho c^2 \int_0^T \left\{ \beta(L,t) v(L,t) - \beta(0,t) v(0,t) \right\} dt.$$

Hence, since $p(l,0) = \bar{p}_0(l)$ and $v(L,t) = u(t)$, we have

$$\int_0^T \int_0^L \beta(l,t) H_2(l,t) dldt = \int_0^L \left\{ \beta(l,T) p(l,T) - \beta(l,0) \bar{p}_0(l) \right\} dl$$

$$- \int_0^T \int_0^L \left\{ \beta_t(l,t) p(l,t) + \rho c^2 \beta_l(l,t) v(l,t) \right\} dldt$$

$$+ \rho c^2 \int_0^T \left\{ \beta(L,t) u(t) - \beta(0,t) v(0,t) \right\} dt.$$

Furthermore, since $H_2(l,t) = 0$ for any pair of state trajectories $p(l,t)$ and $v(l,t)$, we have

$$\int_0^L \left\{ \beta(l,T) p(l,T) - \beta(l,0) \bar{p}_0(l) \right\} dl + \rho c^2 \int_0^T \left\{ \beta(L,t) u(t) - \beta(0,t) v(0,t) \right\} dt$$

$$- \int_0^T \int_0^L \left\{ \beta_t(l,t) p(l,t) + \rho c^2 \beta_l(l,t) v(l,t) \right\} dldt = 0. \tag{17}$$

We now evaluate the gradient of J^N from (9) at a fixed point $\boldsymbol{\sigma} \in \mathbb{R}^{Ns}$, where

$$\boldsymbol{\sigma} = \left[(\boldsymbol{\sigma}^1)^\top, \ldots, (\boldsymbol{\sigma}^N)^\top \right]^\top.$$

Let $\boldsymbol{\theta} \in \mathbb{R}^{Ns}$ be an arbitrary vector partitioned as follows:

$$\boldsymbol{\theta} = \left[(\boldsymbol{\theta}^1)^\top, \ldots, (\boldsymbol{\theta}^N)^\top \right]^\top.$$

We consider the perturbed control vector $\boldsymbol{\sigma} + \epsilon \boldsymbol{\theta}$, where ϵ is a constant of sufficiently small magnitude. Let $p^N(l,t)$, $v^N(l,t)$ denote the state trajectories of (1)-(3) corresponding to $\boldsymbol{\sigma}$, and let $p^{N,\epsilon}(l,t)$, $v^{N,\epsilon}(l,t)$ denote the state trajectories corresponding to $\boldsymbol{\sigma} + \epsilon \boldsymbol{\theta}$. Then

$$p^{N,\epsilon}(l,t) = p^N(l,t) + \epsilon \sum_{k=1}^N \langle \nabla_{\boldsymbol{\sigma}^k} p^N(l,t), \boldsymbol{\theta}^k \rangle + \mathcal{O}(\epsilon^2), \tag{18a}$$

$$v^{N,\epsilon}(l,t) = v^N(l,t) + \epsilon \sum_{k=1}^N \langle \nabla_{\boldsymbol{\sigma}^k} v^N(l,t), \boldsymbol{\theta}^k \rangle + \mathcal{O}(\epsilon^2), \tag{18b}$$

9

where $\mathcal{O}(\epsilon^2)$ denotes higher-order terms such that $\epsilon^{-1}\mathcal{O}(\epsilon^2) \to 0$ as $\epsilon \to 0$. For notational simplicity, define

$$\eta_1(l,t) = \sum_{k=1}^{N} \langle \nabla_{\boldsymbol{\sigma}^k} p^N(l,t), \boldsymbol{\theta}^k \rangle, \quad \eta_2(l,t) = \sum_{k=1}^{N} \langle \nabla_{\boldsymbol{\sigma}^k} v^N(l,t), \boldsymbol{\theta}^k \rangle.$$

Since γ is a positive integer, it follows from the binomial theorem that

$$\left[\frac{p^{N,\epsilon}(l,t) - \hat{p}(l)}{\bar{P}}\right]^{2\gamma} = \left[\frac{p^N(l,t) + \epsilon\eta_1(l,t) - \hat{p}(l)}{\bar{P}}\right]^{2\gamma} + \mathcal{O}(\epsilon^2).$$

Hence, the objective value at $\boldsymbol{\sigma} + \epsilon\boldsymbol{\theta}$ can be expressed as follows:

$$
\begin{aligned}
J^N(\boldsymbol{\sigma} + \epsilon\boldsymbol{\theta}) &= \frac{1}{T}\int_0^T \left[\frac{p^{N,\epsilon}(L,t) - \hat{p}(L)}{\bar{P}}\right]^{2\gamma} dt + \frac{1}{LT}\int_0^T\int_0^L \left[\frac{p^{N,\epsilon}(l,t) - \hat{p}(l)}{\bar{P}}\right]^{2\gamma} dl\, dt \\
&= \frac{1}{T}\int_0^T \left[\frac{p^N(L,t) + \epsilon\eta_1(L,t) - \hat{p}(L)}{\bar{P}}\right]^{2\gamma} dt \\
&\quad + \frac{1}{LT}\int_0^T\int_0^L \left[\frac{p^N(l,t) + \epsilon\eta_1(l,t) - \hat{p}(l)}{\bar{P}}\right]^{2\gamma} dl\, dt + \mathcal{O}(\epsilon^2).
\end{aligned}
$$

By substituting (18a) and (18b) into (16) and (17) (evaluated at $p(l,t) = p^{N,\epsilon}(l,t)$ and $v(l,t) = v^{N,\epsilon}(l,t)$), this equation can be written as

$$
\begin{aligned}
J^N(\boldsymbol{\sigma} + \epsilon\boldsymbol{\theta}) &= \int_0^L \left\{\alpha(l,T)[v^N(l,T) + \epsilon\eta_2(l,T)] - \alpha(l,0)\bar{v}_0(l) + \beta(l,T)[p^N(l,T) + \epsilon\eta_1(l,T)] - \beta(l,0)\bar{p}_0(l)\right\}dl \\
&+ \int_0^T\int_0^L \left\{\frac{1}{LT}\left[\frac{p^N(l,t) + \epsilon\eta_1(l,t) - \hat{p}(l)}{\bar{P}}\right]^{2\gamma} - \left[\frac{1}{\rho}\alpha_l(l,t) + \beta_t(l,t)\right](p^N(l,t) + \epsilon\eta_1(l,t)) \right. \\
&\left. + \frac{f}{2D}\alpha(l,t)(v^N(l,t) + \epsilon\eta_2(l,t))|v^N(l,t) + \epsilon\eta_2(l,t)| - [\alpha_t(l,t) + \rho c^2\beta_l(l,t)](v^N(l,t) + \epsilon\eta_2(l,t))\right\}dl\, dt \\
&+ \int_0^T \left\{\frac{1}{T}\left[\frac{p^N(L,t) + \epsilon\eta_1(L,t) - \hat{p}(L)}{\bar{P}}\right]^{2\gamma} + \frac{1}{\rho}\alpha(L,t)[p^N(L,t) + \epsilon\eta_1(L,t)] \right. \\
&\left. - \frac{P}{\rho}\alpha(0,t) + \rho c^2\beta(L,t)\sum_{k=1}^{N}\varphi_k(t,\boldsymbol{\sigma}^k + \epsilon\boldsymbol{\theta}^k) - \rho c^2\beta(0,t)[v^N(0,t) + \epsilon\eta_2(0,t)]\right\}dt + \mathcal{O}(\epsilon^2).
\end{aligned}
$$

Therefore,

$$
\begin{aligned}
\left.\frac{\partial J^N(\boldsymbol{\sigma} + \epsilon\boldsymbol{\theta})}{\partial\epsilon}\right|_{\epsilon=0} &= \int_0^L \left\{\alpha(l,T)\eta_2(l,T) + \beta(l,T)\eta_1(l,T)\right\}dl - \int_0^T \rho c^2\beta(0,t)\eta_2(0,t)dt \\
&+ \int_0^T\int_0^L \left\{\left[\frac{2\gamma}{LT\bar{P}^{2\gamma}}(p^N(l,t) - \hat{p}(l))^{2\gamma-1} - \frac{1}{\rho}\alpha_l(l,t) - \beta_t(l,t)\right]\eta_1(l,t) \right. \\
&\left. + \left[\frac{f}{D}\alpha(l,t)|v^N(l,t)| - \alpha_t(l,t) - \rho c^2\beta_l(l,t)\right]\eta_2(l,t)\right\}dl\, dt \\
&+ \int_0^T \left\{\left[\frac{2\gamma}{T\bar{P}^{2\gamma}}(p^N(L,t) - \hat{p}(L))^{2\gamma-1} + \frac{1}{\rho}\alpha(L,t)\right]\eta_1(L,t) + \rho c^2\beta(L,t)\sum_{k=1}^{N}\left\langle\frac{\partial\varphi_k(t,\boldsymbol{\sigma}^k)}{\partial\boldsymbol{\sigma}^k}, \boldsymbol{\theta}^k\right\rangle\right\}.
\end{aligned}
$$

10

Recall that $\alpha(l,t)$ and $\beta(l,t)$ are arbitrary Lagrange multiplier functions. Choosing $\alpha(l,t) = \lambda(l,t)$ and $\beta(l,t) = \mu(l,t)$ as the solutions of the costate system (13)-(15) yields

$$\sum_{k=1}^{N}\left\langle\frac{\partial J^N(\boldsymbol{\sigma})}{\partial\boldsymbol{\sigma}^k},\boldsymbol{\theta}^k\right\rangle = \frac{\partial J^N(\boldsymbol{\sigma}+\epsilon\boldsymbol{\theta})}{\partial\epsilon}\bigg|_{\epsilon=0}$$

$$= \rho c^2 \sum_{k=1}^{N}\int_0^T \mu(L,t)\left\langle\frac{\partial\varphi_k(t,\boldsymbol{\sigma}^k)}{\partial\boldsymbol{\sigma}^k},\boldsymbol{\theta}^k\right\rangle dt.$$

Thus, by taking $\boldsymbol{\theta}^k$ as the standard unit basis vectors in $\mathbb{R}^s$, we obtain

$$\nabla_{\boldsymbol{\sigma}^k}J^N(\boldsymbol{\sigma}) = \rho c^2 \int_0^T \mu(L,t)\frac{\partial\varphi_k(t,\boldsymbol{\sigma}^k)}{\partial\boldsymbol{\sigma}^k}dt, \quad k = 1,\ldots,N.$$

This completes the proof. $\qquad\square$

2.2. Piecewise-Linear Control Parameterization

For piecewise-linear control parameterization, we first choose temporal knot points t_k, $k = 0,\ldots,N$, such that

$$0 = t_0 < t_1 < t_2 < \cdots < t_{N-1} < t_N = T.$$

Then the basis functions in (8) are defined as follows:

$$\varphi_k(t,\boldsymbol{\sigma}^k) = (\sigma_1^k t + \sigma_2^k)\chi_{[t_{k-1},t_k)}(t), \quad k = 1,\ldots,N, \tag{19}$$

where σ_1^k and σ_2^k are optimization parameters and

$$\chi_{[t_{k-1},t_k)}(t) = \begin{cases} 1, & \text{if } t \in [t_{k-1},t_k), \\ 0, & \text{otherwise.} \end{cases}$$

The corresponding gradient formulas in Theorem 1 are

$$\nabla_{\sigma_1^k}J^N(\boldsymbol{\sigma}) = \rho c^2 \int_{t_{k-1}}^{t_k} t\mu(L,t)dt, \quad k = 1,\ldots,N,$$

$$\nabla_{\sigma_2^k}J^N(\boldsymbol{\sigma}) = \rho c^2 \int_{t_{k-1}}^{t_k} \mu(L,t)dt, \quad k = 1,\ldots,N.$$

Note that, for pipeline flow control, $u^N(t)$ must be continuous. Thus, we impose the following continuity constraints on the basis functions (19):

$$\sigma_1^{k-1}t_{k-1} + \sigma_2^{k-1} = \sigma_1^k t_{k-1} + \sigma_2^k, \quad k = 2,\ldots,N. \tag{20}$$

11

With the basis functions (19), the initial and terminal conditions in (10) become

$$\sigma_2^1 = u_{\max}, \quad \sigma_1^N T + \sigma_2^N = 0. \tag{21}$$

Moreover, the derivative constraint (11) becomes

$$\sigma_1^k \leq 0, \quad k = 1, \ldots, N. \tag{22}$$

For piecewise-linear basis functions of the form (19), Problem P_0^N can be solved with the additional contraints (20)-(22). These constraints are linear constraints and can be easily handled using standard SQP techniques.

2.3. Piecewise-Quadratic Control Parameterization

For piecewise-quadratic control parameterization, the basis functions in (8) are defined as follows:

$$\varphi_k(t, \boldsymbol{\sigma}^k) = (\sigma_1^k t^2 + \sigma_2^k t + \sigma_3^k)\chi_{[t_{k-1}, t_k)}(t), \quad k = 1, \ldots, N, \tag{23}$$

where t_k, t_{k-1}, and $\chi_{[t_{k-1}, t_k)}(t)$ are as defined in Section 2.2, and σ_1^k, σ_2^k, and σ_3^k are optimization parameters. The corresponding gradient formulas in Theorem 1 are

$$\nabla_{\sigma_1^k} J^N(\boldsymbol{\sigma}) = \rho c^2 \int_{t_{k-1}}^{t_k} t^2 \mu(L, t)dt, \quad k = 1, \ldots, N,$$

$$\nabla_{\sigma_2^k} J^N(\boldsymbol{\sigma}) = \rho c^2 \int_{t_{k-1}}^{t_k} t\mu(L, t)dt, \quad k = 1, \ldots, N,$$

$$\nabla_{\sigma_3^k} J^N(\boldsymbol{\sigma}) = \rho c^2 \int_{t_{k-1}}^{t_k} \mu(L, t)dt, \quad k = 1, \ldots, N.$$

To ensure that $u^N(t)$ with basis functions (23) is continuously differentiable, we impose the following linear constraints:

$$\sigma_1^{k-1} t_{k-1}^2 + \sigma_2^{k-1} t_{k-1} + \sigma_3^{k-1} = \sigma_1^k t_{k-1}^2 + \sigma_2^k t_{k-1} + \sigma_3^k, \quad k = 2, \ldots, N, \tag{24}$$

and

$$2\sigma_1^{k-1} t_{k-1} + \sigma_2^{k-1} = 2\sigma_1^k t_{k-1} + \sigma_2^k, \quad k = 2, \ldots, N. \tag{25}$$

The initial and terminal conditions specified in (10) become

$$\sigma_3^1 = u_{\max}, \quad \sigma_1^N T^2 + \sigma_2^N T + \sigma_3^N = 0. \tag{26}$$

12

Moreover, the derivative constraint (11) becomes

$$2\sigma_1^k t + \sigma_2^k \le 0, \quad t \in [t_{k-1}, t_k), \quad k = 1, \ldots, N.$$

These constraints are clearly equivalent to

$$2\sigma_1^k t_{k-1} + \sigma_2^k \le 0, \quad 2\sigma_1^k t_k + \sigma_2^k \le 0, \quad k = 1, \ldots, N. \tag{27}$$

For piecewise-quadratic control parameterization, Problem P_0^N must be solved with the additional linear constraints (24)-(27).

3. Numerical Implementation

To solve the PDE model (1)-(3), we will use the method of lines to approximate the PDEs by a system of ODEs. This method has proven very effective for solving the nonlinear pipeline transmission PDE model [6, 13]. Let m be an even integer. We partition the pipeline spatial domain into m equally-spaced intervals $[l_{i-1}, l_i]$, $i = 1, \ldots, m$, as shown in Figure 3, where $l_i = i\Delta l$, $i = 0, \ldots, m$, and $\Delta l = L/m$.

Let $v_i^N(t) = v^N(l_i, t)$, $i = 0, \ldots, m$, and $p_i^N(t) = p^N(l_i, t)$, $i = 0, \ldots, m$. Then, using finite differences, we can approximate (1)-(3) by the following system of ODEs:

$$\dot{v}_0^N(t) = \frac{1}{\rho \Delta l}(P - p_1^N(t)) - \frac{f}{2D} v_0^N(t)|v_0^N(t)|, \tag{28a}$$

$$\dot{v}_i^N(t) = \frac{1}{\rho \Delta l}(p_i^N(t) - p_{i+1}^N(t)) - \frac{f}{2D} v_i^N(t)|v_i^N(t)|, \quad i = 1, \ldots, m-1, \tag{28b}$$

$$\dot{p}_i^N(t) = \frac{\rho c^2}{\Delta l}(v_{i-1}^N(t) - v_i^N(t)), \quad i = 1, \ldots, m-1, \tag{28c}$$

$$\dot{p}_m^N(t) = \frac{\rho c^2}{\Delta l}\left\{ v_{m-1}^N(t) - \sum_{k=1}^{N} \varphi_k(t, \boldsymbol{\sigma}^k) \right\}. \tag{28d}$$

From the initial conditions (2), we obtain

$$p_i^N(0) = \bar{p}_0(l_i), \quad v_i^N(0) = \bar{v}_0(l_i), \quad i = 0, \ldots, m. \tag{29}$$

Equations (28) and (29) constitute an initial value problem that can be readily solved (using, for example, Runge-Kutta methods) to determine approximate trajectories for $v^N(l, t)$ and $p^N(l, t)$.
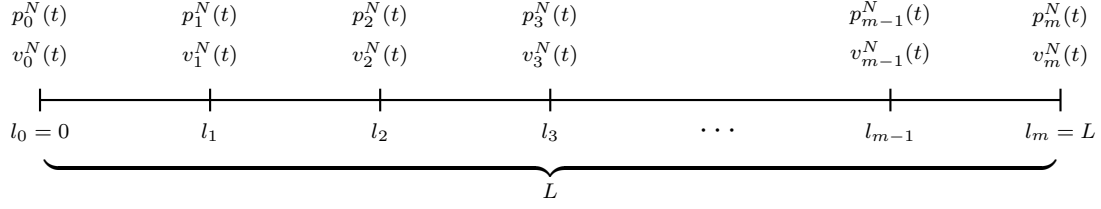
$p_0^N(t)$ $p_1^N(t)$ $p_2^N(t)$ $p_3^N(t)$ $p_{m-1}^N(t)$ $p_m^N(t)$

$v_0^N(t)$ $v_1^N(t)$ $v_2^N(t)$ $v_3^N(t)$ $v_{m-1}^N(t)$ $v_m^N(t)$

$l_0 = 0$ l_1 l_2 l_3 $\cdots$ l_{m-1} $l_m = L$

L

Figure 3: Spatial discretization for the state system using the method of lines, where $p_i^N(t) = p^N(l_i, t)$ and $v_i^N(t) = v^N(l_i, t)$

$\mu_0(t)$ $\mu_1(t)$ $\mu_2(t)$ $\mu_3(t)$ $\mu_{m-1}(t)$ $\mu_m(t)$

$\lambda_0(t)$ $\lambda_1(t)$ $\lambda_2(t)$ $\lambda_3(t)$ $\lambda_{m-1}(t)$ $\lambda_m(t)$

$l_0 = 0$ l_1 l_2 l_3 $\cdots$ l_{m-1} $l_m = L$
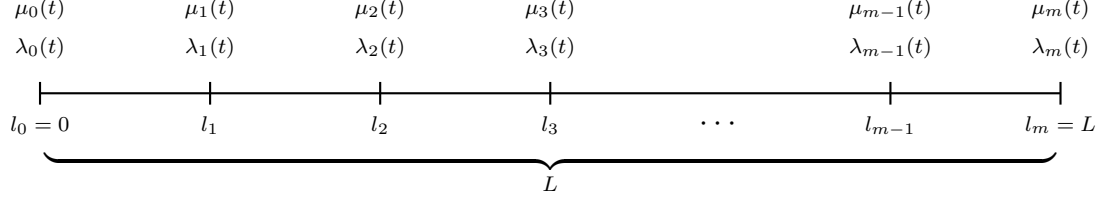
L

Figure 4: Spatial discretization for the costate system using the method of lines, where $\mu_i(t) = \mu(l_i, t)$ and $\lambda_i(t) = \lambda(l_i, t)$

Now, let $\lambda_i(t) = \lambda(l_i, t)$, $i = 0, \ldots, m$, and $\mu_i(t) = \mu(l_i, t)$, $i = 0, \ldots, m$, as shown in Figure 4. In a similar manner to the state system, we can derive the following approximate ODEs for the costate system:

$$\dot{\lambda}_0(t) = \frac{f}{D}\lambda_0(t)|v_0^N(t)| - \frac{\rho c^2}{\Delta l}\mu_1(t), \tag{30a}$$

$$\dot{\lambda}_i(t) = \frac{f}{D}\lambda_i(t)|v_i^N(t)| - \frac{\rho c^2}{\Delta l}(\mu_{i+1}(t) - \mu_i(t)), \quad i = 1, \ldots, m-1, \tag{30b}$$

$$\dot{\mu}_i(t) = \frac{2\gamma}{LT\bar{P}^{2\gamma}}(p_i^N(t) - \hat{p}(l_i))^{2\gamma - 1} - \frac{1}{\rho\Delta l}(\lambda_i(t) - \lambda_{i-1}(t)), \quad i = 1, \ldots, m-1, \tag{30c}$$

$$\dot{\mu}_m(t) = \frac{2\gamma}{T\bar{P}^{2\gamma}}\left[\frac{1}{\Delta l} + \frac{1}{L}\right](p_m^N(t) - \hat{p}(L))^{2\gamma - 1} + \frac{1}{\rho\Delta l}\lambda_{m-1}(t). \tag{30d}$$

Moreover, the costate terminal conditions (15) imply

$$\mu_i(T) = \lambda_i(T) = 0, \quad i = 0, \ldots, m. \tag{31}$$

Given the state trajectories $p_i^N(t)$ and $v_i^N(t)$, $i = 0, \ldots, m$, the costate ODEs (30) can be solved backward in time starting with the terminal conditions (31). To solve Problem P_0^N, the key point is to compute the objective function (9) and its gradient (12). Once we have obtained $p_i^N(t), v_i^N(t), \lambda_i(t)$ and $\mu_i(t)$, $i = 0, \ldots, m$, we can calculate the objective function and its gradient by applying the Composite Simpson's rule [14]. Using

this approach, standard gradient-based optimization techniques can be applied to solve Problem P_0^N numerically.

4. Numerical Simulations

For numerical testing, we implemented three solution methods in MATLAB: the new CP-PDE approach described in Sections 2 and 3, the previous CP-ODE approach described in [8], and the particle swarm optimization (PSO) method described in [26]. These MATLAB implementations use ODE23 to solve the differential equations. The CP-PDE and CP-ODE implementations use the intrinsic subroutine FMINCON to perform the optimization steps. The PSO implementation incorporates the constraints (20)-(22) and (24)-(27) into the objective using a penalty function.

Our test scenario is based on a 200 meter stainless steel pipeline connected to a reservoir of height 20 meters [8, 38]. The corresponding parameters in the PDE model (1)-(3) are: $L = 200$ m, $D = 100$ mm, $\rho = 1000$ kg/m^3, $c = 1200$ m/s, $f = 0.03$ and $P = 2 \times 10^5$ Pa. As in [8], we assume that the pipeline fluid flow is initially in the steady state with constant velocity $\bar{v}_0(l) = 2$ m/s. Thus, from (1a),

$$\frac{1}{\rho}\frac{\partial \bar{p}_0(l)}{\partial l} + \frac{2f}{D} = 0.$$

Since $\bar{p}_0(0) = P$, this differential equation can be solved to yield

$$\bar{p}_0(l) = P - \frac{2\rho f}{D}l.$$

The maximum flow velocity is $u_{\max} = 2$ m/s and the terminal time is $T = 10$ seconds. Moreover, as suggested in references [4, 8], we choose $\gamma = 2$, $\bar{P} = 1 \times 10^5$ Pa, and $\hat{p}(l) = P = 2 \times 10^5$ Pa in the objective function (7), since once the valve is fully closed, the pressure along the pipeline is the same as the pressure generated by the reservoir.

4.1. Piecewise-Linear Control Parameterization

We applied piecewise-linear control parameterization (see Section 2.2) to obtain the corresponding Problem P_0^N. This approximate problem was then solved using the CP-PDE, CP-ODE, and PSO methods. Table 1 gives the corresponding computation times and optimal objective values for $N = 10$ temporal subintervals and
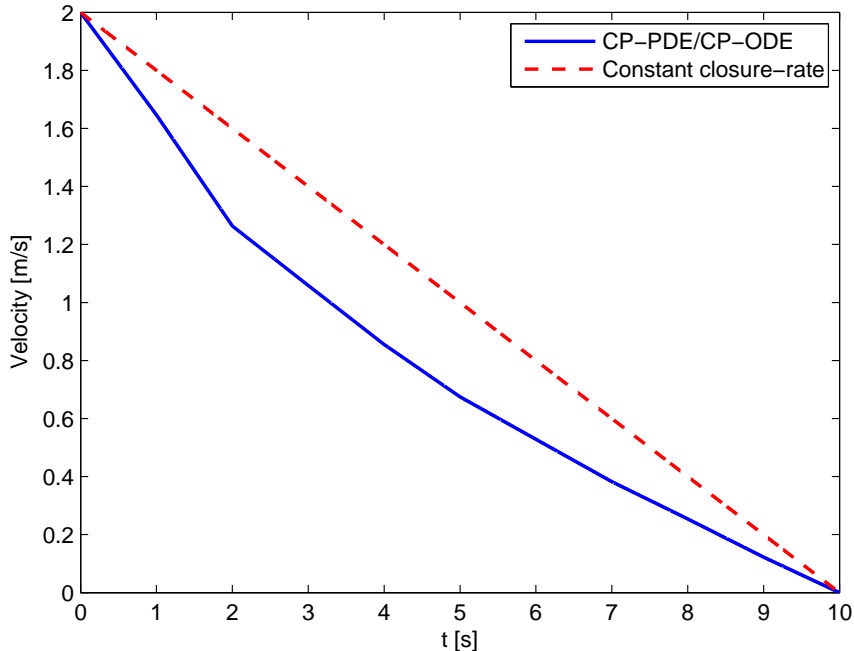
15

Figure 5: Optimal piecewise-linear control for $N = 10$ and $m = 24$ (note that the controls from CP-PDE and CP-ODE are almost identical)

$m \in \{16, 18, 20, 22, 24\}$ spatial subintervals. For each method, the initial guess for the control parameters was chosen as $(\sigma_1^k, \sigma_2^k) = (-0.2, 2)$, $k = 1, \ldots, N$. This initial guess corresponds to the "constant closure-rate" control strategy defined by

$$u(t) = u_{\max} - \frac{u_{\max}}{T} t = 2 - \frac{1}{5} t.$$

For this example, CP-PDE, CP-ODE and the PSO algorithm produce similar results in terms of optimal objective value, but CP-PDE converges much quicker than both CP-ODE and PSO. Indeed, as the number of spatial intervals is increased, the computation time for CP-PDE tends to increase at a much slower rate than the other methods. In addition, the objective value corresponding to the constant closure-rate strategy is 6.8555×10^{-2}, which is 166% higher than the best objective value in Table 1. The optimal piecewise-linear controls produced by CP-PDE and CP-ODE are virtually identical. We plot the optimal piecewise-linear control for $m = 24$ in Figure 5, along with the constant closure-rate strategy. The corresponding pressure profiles at the pipeline terminus are shown in Figure 6. Finally, Table 2 gives the optimal control parameters for CP-PDE with $m = 24$.

16

Method	m	CPU Time [s]	Objective Value
CP-PDE	16	158	2.6708×10^{-2}
CP-ODE	16	526	2.6687×10^{-2}
PSO	16	1281	2.6721×10^{-2}
CP-PDE	18	165	2.6420×10^{-2}
CP-ODE	18	804	2.6405×10^{-2}
PSO	18	1599	2.6438×10^{-2}
CP-PDE	20	172	2.6161×10^{-2}
CP-ODE	20	930	2.6160×10^{-2}
PSO	20	1856	2.6183×10^{-2}
CP-PDE	22	182	2.5937×10^{-2}
CP-ODE	22	992	2.5944×10^{-2}
PSO	22	2042	2.5931×10^{-2}
CP-PDE	24	192	2.5750×10^{-2}
CP-ODE	24	1339	2.5752×10^{-2}
PSO	24	2096	2.5738×10^{-2}

Table 1: Comparing the CP-PDE, CP-ODE, and PSO methods with piecewise-linear control parameterization

k	1	2	3	4	5
σ_1^k	-0.3536	-0.3827	-0.2049	-0.2034	-0.1805
σ_2^k	2.0000	2.0291	1.6736	1.6690	1.5773
k	6	7	8	9	10
σ_1^k	-0.1464	-0.1460	-0.1284	-0.1317	-0.1223
σ_2^k	1.4070	1.4045	1.2817	1.3078	1.2235

Table 2: Optimal control parameters for CP-PDE with piecewise-linear control parameterization, $N = 10$ temporal subintervals, and $m = 24$ spatial subintervals
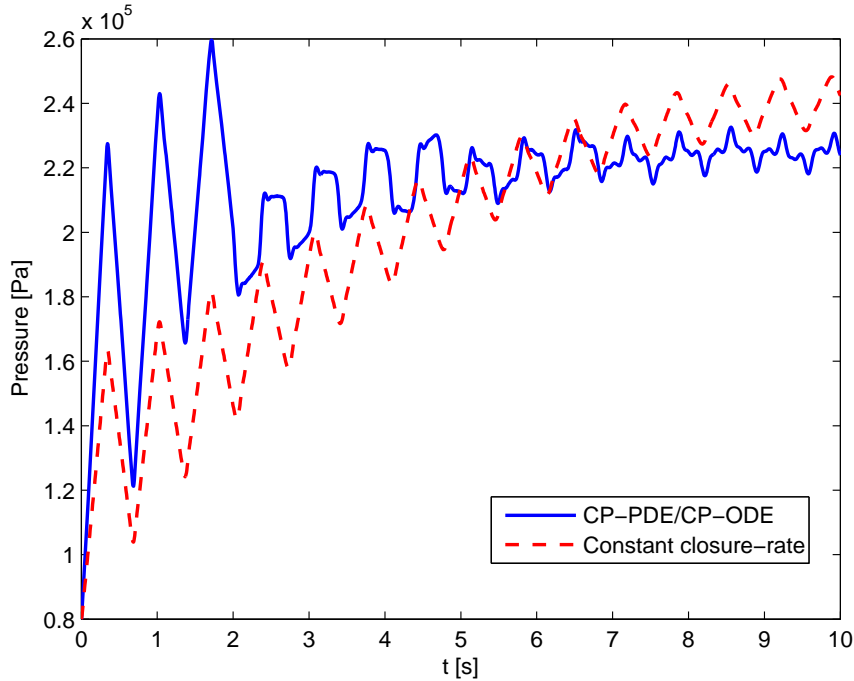
Figure 6: Pressure at the pipeline terminus corresponding to the boundary controls in Figure 5

4.2. Piecewise-Quadratic Control Parameterization

We also applied piecewise-quadratic control parameterization (see Section 2.3) to solve the boundary control problem. For CP-PDE, we considered both smooth and non-smooth piecewise-quadratic boundary controls. The smooth boundary control is obtained by solving Problem P_0^N with constraints (24)-(27); the non-smooth boundary control is obtained by including constraints (24), (26), (27) and omitting (25). Note that CP-ODE is only capable of producing smooth piecewise-quadratic controls. The computation times and optimal objective function values for $N = 10$ and $m \in \{16, 18, 20, 22, 24\}$ are reported in Table 3. As with piecewise-linear control parameterization, the computation times for CP-PDE are much less than those for CP-ODE and PSO. The results also suggest that the non-smooth piecewise-quadratic approximation scheme yields less pressure fluctuation. The optimal piecewise-quadratic boundary controls for $N = 10$ and $m = 24$ are shown in Figure 7 and the corresponding pressure profiles at the pipeline terminus are shown in Figure 8. Table 4 and 5 give the optimal control parameters produced by CP-PDE (smooth and non-smooth boundary control) for $N = 10$ and $m = 24$, respectively. Finally, Figures 9-12 show the pressure evolutions along the pipeline for the constant closure-rate, optimal piecewise-linear, and optimal
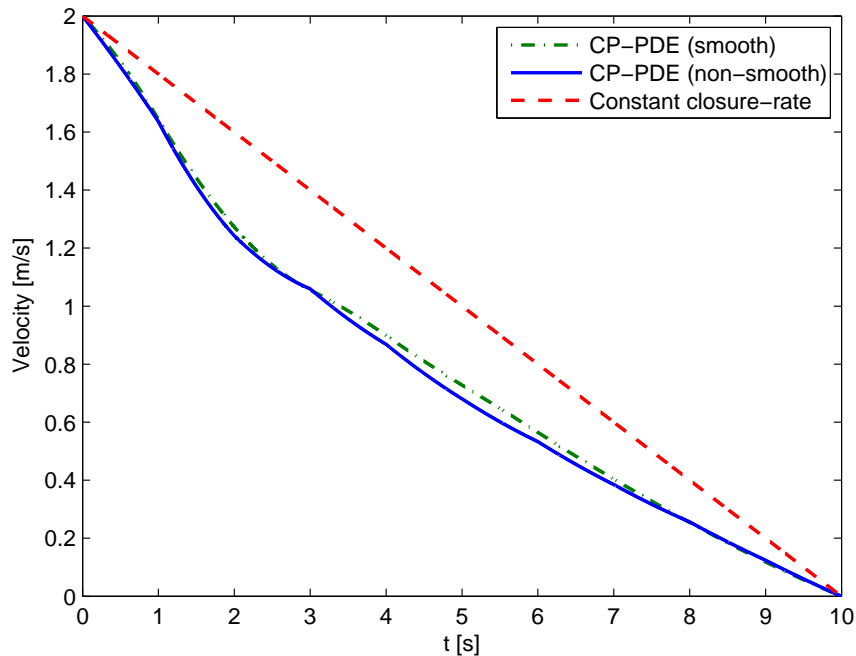
18

Figure 7: Optimal piecewise-quadratic controls for $N = 10$ and $m = 24$

piecewise-quadratic control strategies.

5. Conclusion

In this paper, we have proposed a new computational method for active boundary control of water hammer in fluid pipelines. The method involves parameterizing the boundary control function in terms of a finite number of decision parameters, each of which must be chosen optimally to minimize the deviation between actual and desired pressure profiles. We call this approach the CP-PDE approach because it involves applying control parameterization directly to the hyperbolic PDE system describing the pipeline fluid flow. In contrast, the CP-ODE approach proposed in [8] involves applying control parameterization to an approximate system of ODEs, instead of the original PDE model. The numerical results in Section 4 show that CP-PDE and CP-ODE produce almost identical control strategies, but CP-PDE is far more efficient at computing the optimal solution. This is because CP-PDE only requires solving $4m$ ODEs (see Section 3), much less than the $2mN$ ODEs required for CP-ODE (see reference [8]). The CP-PDE approach is also far more efficient than the PSO method for the examples in Section 4. We conclude by mentioning an interesting link between Problem P_0 and the

19

Method	m	CPU Time [s]	Objective Value
CP-PDE (smooth)	16	223	2.7408×10^{-2}
CP-PDE (non-smooth)	16	302	2.5027×10^{-2}
CP-ODE	16	622	2.6571×10^{-2}
PSO	16	1319	2.9461×10^{-2}
CP-PDE (smooth)	18	231	2.7299×10^{-2}
CP-PDE (non-smooth)	18	306	2.4804×10^{-2}
CP-ODE	18	638	2.6550×10^{-2}
PSO	18	1444	2.927×10^{-2}
CP-PDE (smooth)	20	239	2.7254×10^{-2}
CP-PDE (non-smooth)	20	332	2.4542×10^{-2}
CP-ODE	20	923	2.6539×10^{-2}
PSO	20	2249	2.8867×10^{-2}
CP-PDE (smooth)	22	252	2.7211×10^{-2}
CP-PDE (non-smooth)	22	356	2.4378×10^{-2}
CP-ODE	22	995	2.6532×10^{-2}
PSO	22	2567	2.8841×10^{-2}
CP-PDE (smooth)	24	276	2.7181×10^{-2}
CP-PDE (non-smooth)	24	441	2.4098×10^{-2}
CP-ODE	24	1774	2.6522×10^{-2}
PSO	24	2861	2.8819×10^{-2}

Table 3: Comparing the CP-PDE, CP-ODE, and PSO methods with piecewise-quadratic control parameterization

k	1	2	3	4	5
σ_1^k	-0.0814	0.0677	0.0842	-0.0241	0.0126
σ_2^k	-0.2772	-0.5754	-0.6415	-0.0083	-0.2853
σ_3^k	2.0000	2.1491	2.2152	1.2404	1.8277
k	6	7	8	9	10
σ_1^k	0.0032	0.0066	0.0057	0.0085	0.0095
σ_2^k	-0.1269	-0.2444	-0.2330	-0.2776	-0.2945
σ_3^k	1.4317	1.7843	1.7443	1.9228	1.9986

Table 4: Optimal control parameters for CP-PDE with piecewise-quadratic control parameterization (smooth), $N = 10$ temporal subintervals, and $m = 24$ spatial subintervals

k	1	2	3	4	5
σ_1^k	-0.0319	0.1117	0.1045	-0.0165	0.0383
σ_2^k	-0.3321	-0.7349	-0.7145	-0.0743	-0.5294
σ_3^k	2.0000	2.2593	2.2490	1.4151	2.3586
k	6	7	8	9	10
σ_1^k	0.0122	0.0183	0.0119	0.0180	0.0096
σ_2^k	-0.2811	-0.3826	-0.3081	-0.3149	-0.2980
σ_3^k	1.7695	2.1586	1.9479	2.0719	2.0210

Table 5: Optimal control parameters for CP-PDE with piecewise-quadratic control parameterization (non-smooth), $N = 10$ temporal subintervals, and $m = 24$ spatial subintervals
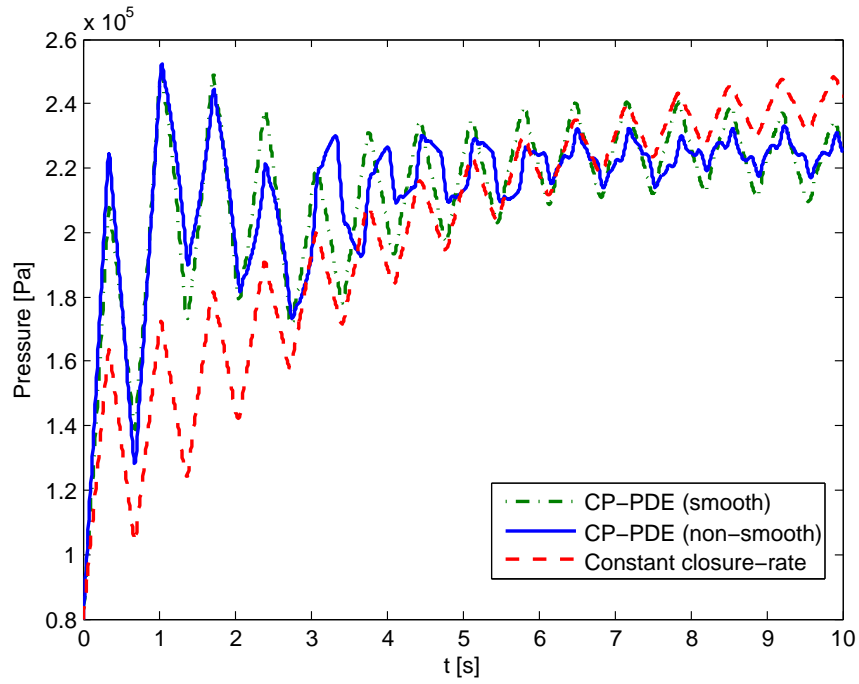
Figure 8: Pressure at the pipeline terminus corresponding to the boundary controls in Figure 7
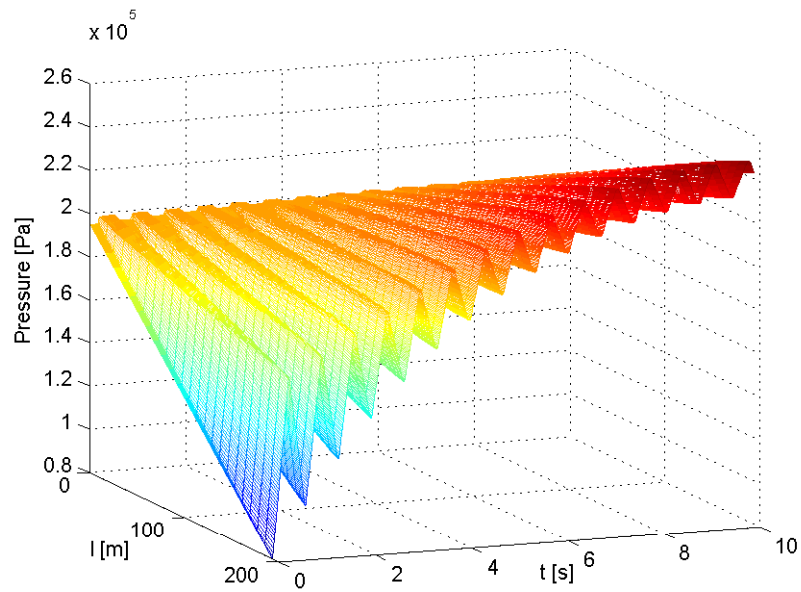

Figure 9: Pressure evolution corresponding to the constant closure-rate control strategy
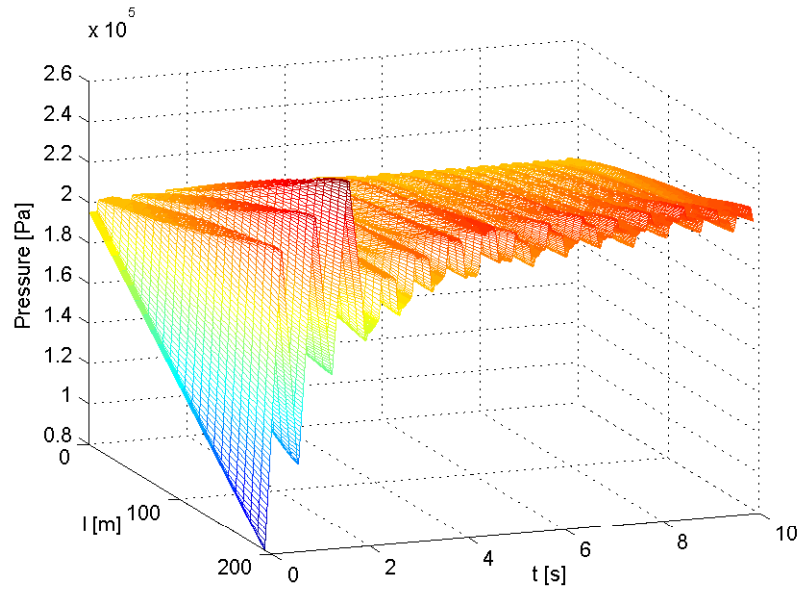
Figure 10: Pressure evolution corresponding to the optimal piecewise-linear control strategy for $N = 10$ and $m = 24$ (CP-PDE approach)
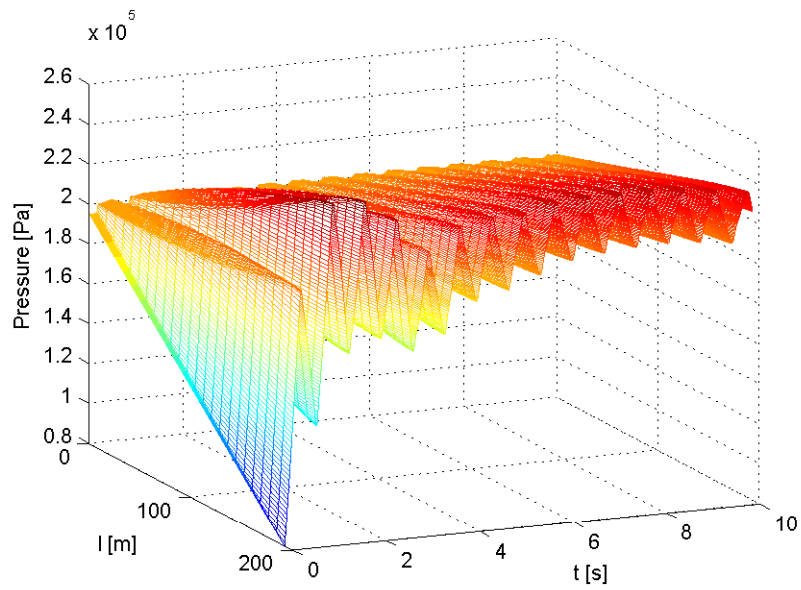

Figure 11: Pressure evolution corresponding to the smooth piecewise-quadratic control strategy for $N = 10$ and $m = 24$ (CP-PDE approach)
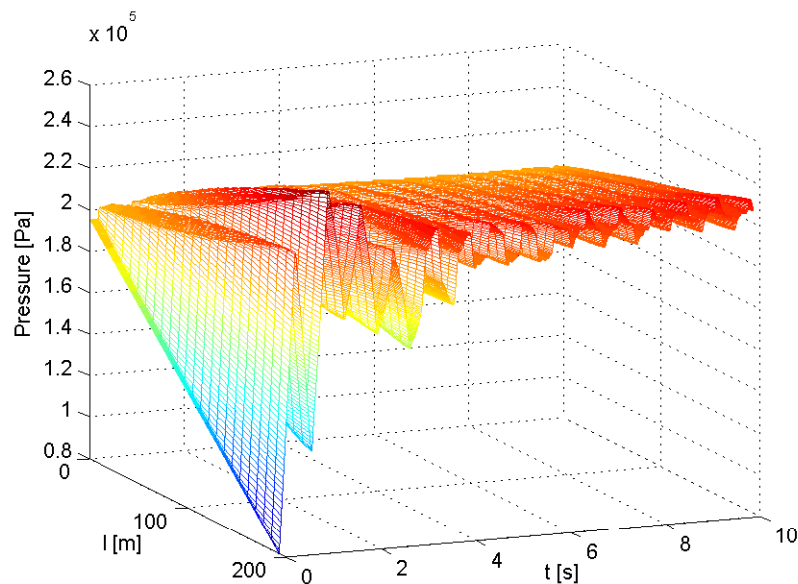
Figure 12: Pressure evolution corresponding to the non-smooth piecewise-quadratic control strategy for $N = 10$ and $m = 24$ (CP-PDE approach)

class of optimal control problems considered in reference [23], which incorporate penalties on the total variation of the control signal. The aim in such problems is to minimize control fluctuation, thereby reducing wear and tear on the system. We speculate that this "minimal variation" framework could indeed be applied to water hammer suppression by minimizing the total variation of the pressure profile. The aim in this context would be to eliminate highly volatile pressure profiles that could cause serious damage to the pipeline structure. This direction will be explored in future work. Another direction to pursue is real-time implementation of the open-loop parameterized control by suitable scheduling of the valve operation sequences. It is possible to use feedback control techniques to track the optimal control target if the external perturbations are reasonably small. Another option is FPGA-based (Field Programmable Gate Array) implementation combined with model reduction techniques [37].

References

[1] O. M. Aamo and M. Krstic. *Flow Control by Feedback: Stabilization and Mixing.* Springer, 2002.

[2] I. Aksikas, J. J. Winkin, and D. Dochain. Asymptotic stability of infinite-dimensional semilinear systems: Application to a nonisothermal reactor. *Systems and Control Letters*, 56(2):122–132, 2007.

[3] K. H. Asli, F. B. O. Naghiyev, and A. K. Haghi. Some aspects of physical and numerical modeling of water hammer in pipelines. *Nonlinear Dynamics*, 60(4):677–701, 2010.

[4] G. A. Atanov, E. G. Evseeva, and P. A. Work. Variational problem of water-level stabilization in open channels. *Journal of Hydraulic Engineering*, 124(1):50–54, 1998.

[5] A. Balogh, O. M. Aamo, and M. Krstic. Optimal mixing enhancement in 3D pipe flow. *IEEE Transactions on Control Systems Technology*, 13(1):27–41, 2005.

[6] O. S. Balogun, M. Hubbard, and J. J. DeVries. Automatic control of canal flow using linear quadratic regulator theory. *Journal of Hydraulic Engineering*, 114(1):75–102, 1988.

[7] A. Bergnt, A. R. Simpson, and E. Sijamhodzic. Water hammer analysis of pumping systems for control of water in underground mines. In *Proceedings of the Fourth International Mine Water Association Congress*, Ljubljana, Slovenia, September 1991.

[8] T. Chen, Z. Ren, C. Xu, and R. Loxton. Optimal boundary control for water hammer suppression in fluid transmission pipelines. *Computers and Mathematics with Applications*, 69(4):275–290, 2015.

[9] J. M. Coron, B. d'Andrea Novel, and G. Bastin. A strict Lyapunov function for boundary control of hyperbolic systems of conservation laws. *IEEE Transactions on Automatic Control*, 52(1):2–11, 2007.

[10] M. Dick, M. Gugat, and G. Leugering. Classical solutions and feedback stabilization for the gas flow in a sequence of pipes. *Networks and Heterogeneous Media*, 5(4):691–709, 2010.

[11] V. Dos Santos and C. Prieur. Boundary control of open channels with numerical and experimental validations. *IEEE Transactions on Control Systems Technology*, 16(6):1252–1264, 2008.

[12] W. Erath, B. Nowotny, and J. Maetz. Modelling the fluid structure interaction produced by a water hammer during shutdown of high-pressure pumps. *Nuclear Engineering and Design*, 193(3):283–296, 1999.

[13] D. Georges. Nonlinear model identification and state-observer design for water distribution systems. In *Proceedings of the International Conference on Control*, Coventry, UK, March 1994.

[14] C. F. Gerald and P. O. Wheatley. *Numerical Analysis*. Addison-Wesley, 2003.

[15] M. S. Ghidaoui. On the fundamental equations of water hammer. *Urban Water Journal*, 1(2):71–83, 2004.

[16] S. Ki Ooi, M. P. M. Krutzen, and E. Weyer. On physical and data driven modelling of irrigation channels. *Control Engineering Practice*, 13(4):461–471, 2005.

[17] R. Lecourt and J. Steelant. Experimental investigation of water hammer in simplified feed lines of satellite propulsion systems. *Journal of Propulsion and Power*, 23(6):1214–1224, 2007.

[18] T. S. Lee and K. L. Ngoh. Air entrainment effects on the pressure transients of pumping systems with weir discharge chamber. *Journal of Fluids Engineering*, 124(4):1034–1043, 2002.

[19] Q. Lin, R. Loxton, and K. L. Teo. The control parameterization method for nonlinear optimal control: A survey. *Journal of Industrial and Management Optimization*, 10(1):275–309, 2014.

[20] Q. Lin, R. Loxton, K. L. Teo, Y. H. Wu, and C. Yu. A new exact penalty method for semi-infinite programming problems. *Journal of Computational and Applied Mathematics*, 261:271–286, 2014.

[21] X. Litrico, V. Fromion, J. P. Baume, C. Arranja, and M. Rijo. Experimental validation of a methodology to control irrigation canals based on Saint-Venant equations. *Control Engineering Practice*, 13(11):1425–1437, 2005.

[22] X. G. Liu, Y. Q. Hu, J. H. Feng, and K. Liu. A novel penalty approach for nonlinear dynamic optimization problems with inequality path constraints. *IEEE Transactions on Automatic Control*, 59(10):2863–2867, 2014.

[23] R. Loxton, Q. Lin, and K. L. Teo. Minimizing control variation in nonlinear optimal control. *Automatica*, 49(9):2652–2664, 2013.

[24] R. C. Loxton, K. L. Teo, V. Rehbock, and K. F. C. Yiu. Optimal control problems with a continuous inequality constraint on the state and the control. *Automatica*, 45(10):2250–2257, 2009.

[25] I. Mareels, E. Weyer, S. K. Ooi, M. Cantoni, Y. Li, and G. Nair. Systems engineering for irrigation systems: Successes and challenges. *Annual Reviews in Control*, 29(2):191–204, 2005.

[26] I. Montalvo, J. Izquierdo, R. Pérez, and M. M. Tung. Particle swarm optimization applied to the design of water supply systems. *Computers and Mathematics with Applications*, 56(3):769–776, 2008.

[27] S. J. Moura and H. K. Fathy. Optimal boundary control & estimation of diffusion-reaction PDEs. In *Proceedings of the 2011 American Control Conference*, San Francisco, USA, July 2011.

[28] T. J. Pedley. *Fluid Mechanics of Large Blood Vessels*. Cambridge University Press, 1980.

[29] V. Pham, D. Georges, and G. Besançon. Predictive control with guaranteed stability for water hammer equations. *IEEE Transactions on Automatic Control*, 59(2):465–470, 2014.

[30] C. Schmitt, G. Pluvinage, E. Hadj-Taieb, and R. Akid. Water pipeline failure

due to water hammer effects. *Fatigue and Fracture of Engineering Materials and Structures*, 29(12):1075–1082, 2006.

[31] K. L. Teo, C. J. Goh, and K. H. Wong. *A Unified Computational Approach to Optimal Control Problems*. Longman Scientific and Technical, 1991.

[32] W. X. Tian, G. Su, G. P. Wang, S. Z. Qiu, and Z. J. Xiao. Numerical simulation and optimization on valve-induced water hammer characteristics for parallel pump feedwater system. *Annals of Nuclear Energy*, 35(12):2280–2287, 2008.

[33] R. Vazquez, M. Krstic, and J. M. Coron. Backstepping boundary stabilization and state estimation of a 2×2 linear hyperbolic system. In *Proceedings of the 50th IEEE Conference on Decision and Control and European Control Conference*, Orlando, USA, December 2011.

[34] R. Weinstock. *Calculus of Variations*. Courier Dover Publications, 2012.

[35] E. B. Wylie, V. L. Streeter, and L. Suo. *Fluid Transients in Systems*. Prentice Hall, 1993.

[36] C. Xu, Y. Dong, Z. Ren, H. Jiang, and X. Yu. Sensor deployment for pipeline leakage detection via optimal boundary control strategies. *Journal of Industrial and Management Optimization*, 11(1):199–216, 2015.

[37] N. Yang, D. Li, J. Zhang, and Y. Xi. Model predictive controller design and implementation on FPGA with application to motor servo system. *Control Engineering Practice*, 20(11):1229–1235, 2012.

[38] X. Zhao, X. Y. Zhang, M. D. Zhao, and H. Y. Dong. *Hydraulics*. China Electric Power Press, 2009.